Author Version: *J. Geol. Soc. India, vol.86(1); 2015; 41-51*

Mineral chemistry and alteration characteristics of spinel in serpentinised peridotites from the Northern Central Indian Ridge

RANADIP BANERJEE[1] , DWIJESH RAY[2] and TERUAKI ISHII[3]

1 National Institute of Oceanography, Dona Paula, Goa 403004, India

2 PLANEX, Physical Research Laboratory, Ahmedabad 380009, India 3 Fukada Geological Institute, Honkomagome, Tokyo 113-0021, Japan

Email: ocean1@rediffmail.com; dwijesh@rediffmail.com

Abstract

Serpentinites (frequently cross cut by gabbroic dikelet), collected from Northern Central Indian Ridge (NCIR), Indian Ocean, contain both Cr-rich (Group I) and Cr-poor (Group II) variety of spinel. Based on mineralogy they can be classified as non-residual and residual spinel, respectively. While, non residual spinel (TiO_2 up to 0.5 wt %; Group I) display the evidences of peridotite-gabbro interaction, residual spinel (TiO_2<0.1 wt%; Cr# ~24; Group II), suggests intermediate degree of partial melting (~10%) of mantle peridotite, which falls between most depleted mantle peridotite (~15%) and most fertile peridotite (~5%). Alteration of spinel porphyroclast is conceded by the presence of relict fresh interior, intermediate ferritchromit zone and secondary magnetite at the margins. Due to the effect of serpentinisation, marginal areas of spinel porphyroclasts display increasing Fe, but decreasing Al and Mg, while their Cr content remain unaffected throughout the spinel.

Keywords: Mineral chemistry, Spinel, Serpentinites, Alteration characteristics, Central Indian Ridge

Introduction

Spinel composition is a useful tracer of melting process in residual peridotites as they reflect the degree of mantle melting in producing the chromium spinel-bearing peridotites (Dick and Bullen, 1984; Arai, 1994, Hellebrand et al., 2002). Previous studies on the residual spinel chemistry were mainly focused on those from the different segments of Mid-Atlantic Ridge (MAR), Hess Deep, East Pacific Rise (EPR), Southwest India Ridge (SWIR) and even from the slowest spreading Gakkel ridge (Arai, 1994; Hellebrand et al., 2002; Ross and Elthon, 1997; Ghosh et al., 1996; Dick, 1989; Bach et al., 2004, 2006; Seyler et al., 2003). Earlier studies on petrology of Northern Central Indian Ridge (NCIR) has been focused primarily on the geochemical characterisation of basalts, magmatic evolutionary processes and isotopic geochemistry, to identify igneous processes and to explain mantle characteristics beneath the northern Indian Ocean (Mahoney et al., 1989; Natland, 1991; Rehkämper and Hofmann, 1997; Ray et al., 2007, 2011, 2013). However, details regarding geochemical characters and formation process of mantle peridotite and serpentinites from NCIR are sparsely available in literature (Engel and Fisher, 1975; Ray et al., 2009). A few studies carried out recently to explain the degree of partial melting and behavior of mobile elements during serpentinisation processes, are mostly from southern part of Central Indian Ridge (CIR) (Hellebrand et al., 2002; Morishita et al., 2009), while the NCIR remains unexplored.

Spinel, an important accessory mineral in mantle peridotite, is generally more resistant to alteration and or metamorphism as compared to olivine, plagioclase and pyroxene. Therefore, spinel could be a useful tracer to examine the mineral-textural variations and the extent of alteration during serpentinisation of mantle peridotite. Additionally, the degree of partial melting processes can also be assessed using the mineral chemistry of unaltered spinel core. In this paper, we discussed the nature of partial melting of NCIR mantle peridotites and the alteration processes affecting the composition of spinel during serpentinisation of the mantle peridotites.

Geological setting of study area

The NCIR (~26–38 mm/yr, full spreading rate, Kamesh Raju et al., 2012), one of the poorly constrained mid-ocean ridge system, has important implications on the dynamics of slow sea-floor spreading. Between 5° to 10°S and 68° to 70°E, NCIR geometry is

characterised by short ridge segments and long transform faults. The rock types from all these different ridge segments have shown magma-rich and magma-poor phases of extension vis-à-vis accretionary processes (Drolia et al., 2003; Kamesh Raju et al., 2012). Approximately 1200 kg of serpentinised peridotites were collected using chain-bag dredge during a cruise of Ocean Research Vessel Sagar Kanya (cruise number SK/195) in the year 2003 from NCIR at 6º39'S, 68º32'E (water depth of 2800 m) (Fig. 1). Representative samples (Table 1) from this collection (n=15) were studied for understanding the mineral chemistry of spinel. From these samples, 102 spinel grains were analyzed (Table 3) to study their mineral composition and from them data of 18 grains (Table 2) are reported here. The sampling location was at an inside corner high at ridge-transform intersection (RTI), south of the Vityaz transform fault (at 6ºS). At this location, the half spreading rate (19 mm/yr) is similar to that of southern Mid-Atlantic Ridge (MAR) (Drolia and DeMets, 2006).

Samples and Analytical techniques

Majority (~80%) of the dredged serpentinised peridotites are free from any gabbroic dikelet intrusion, while remaining (20%) peridotites are intruded by gabbroic dikelet. Petrographic studies of rock thin sections were carried out to understand the variations in mineral textural pattern and mineral association. Back Scattered Electron (BSE) imaging, X-ray mapping and mineral compositions were obtained using a EPMA (model JEOL JXA-8900R) with five wavelength dispersive spectrometers (WDS) at Ocean Research Institute, University of Tokyo. Silicate and oxide minerals were analysed using a focused beam. Natural and synthetic standards were employed for calibration. The element and their corresponding mineral standards are as follows: Na (Jadeite), K (Orthoclase), Mg (Olivine), Si (Diopside), Ca (Wollastonite), Mn (Rhodonite), Fe (Almandine), Ti (TiO_2), Cr (Cr_2O_3), P (Apatite), Co (Co metal), Ni (Ni metal) and S (Pyrite). Glass standard NIST 610 was used during the analyses, and the results demonstrate a precision better than ±5%. The operating conditions were 15 keV accelerating voltage, 50 nA specimen current and <10 μm beam diameter. The counting time was kept at 7 seconds for Na, K and Si, and 10 seconds for Mg, Al, Ca, Ti, Cr, Mn, and Fe. The data were ZAF corrected. Identification of serpentine polymorphs was performed by X-ray diffractogram (XRD, model Philips 1840) at National Institute of Oceanography, Goa, India. Operating conditions for XRD analyses was 40 kV with an operating current of 22 mA.

Results

Petrography

Table 1 summarises the brief petrographic descriptions of serpentinised peridotites, with and without intrusion by gabbroic dikelets. In hand specimen, peridotites are intensely serpentinised and sometimes crosscut by gabbroic dikelets (which are also altered). The effect of serpentinisation is pervasive and only a few relict primary minerals (e.g. spinel) survived. Olivine and orthopyroxene were completely pseudomorphed by serpentine as exemplified by 'mesh' and 'bastite' textures, respectively. These textures occupy almost 60 vol%, followed by serpentine veins (20 vol%), magnetite (10 vol%) and spinel (10 vol%). In 'mesh' texture, serpentine replaces the olivine and in this process the original outline of olivine is obliterated, forming concentric growth of serpentine and magnetite. By contrast, in 'bastite' the original outline of the pyroxene is generally retained even after their composition is replaced by serpentine (Figs. 2a, b). Adjacent areas of gabbroic dikelets are altered to chlorite (alteration of plagioclase) and actinolite (but rarely to edenite). Magnetites sometime occur along the peripheral rim of spinel grains (Figs. 3a, b) as an alteration product. The reddish brown spinel grains show variable morphology, e.g. blocky with slightly altered rim and fresh core (Fig. 3a), anhedral (Fig. 3c), worm-vein like or 'holly-leaf' and vermicular shaped (Fig. 3d), irregularly rounded (Fig. 3e), and euhedral (Fig. 3f). At some places, a few large fractured spinel porphyroclasts occur with traces of serpentinisation along those fractures, in close association with 'bastite' (Fig. 3b). Occasionally, euhedral spinel grains occur within or even adjacent to the actinolite vein. Chlorite (as altered product of plagioclase) veins often occur within the bastite (Fig. 3f). Actinolite vein and spinel also occur in close association with the late stage carbonate vein within the peridotites (Figs. 4 a,b,c). XRD analyses of bulk serpentine reveal distinct peaks for 1T-lizardite (PDF No. 11-386), 2M chrysotile (PDF No 31-808), and orthochrysotile (PDF No. 25-645). Magnetites are present outlining the mesh periphery, at the central part or at the margins of the serpentine veins.

Mineral chemistry

BSE image (Fig. 5) of a porphyroclastic spinel with highly irregular outline shows the effects of alteration restricted to the inner fractures. In order to assess the degree of compositional zoning imposed due to 'sub solidus re-equilibration' or 'variable intensity of

serpentinisation' several electron microprobe line profiles were run across the spinel grains. While, within the fresh region, there is a compositional uniformity, the outer margins are mostly enriched in Fe contents as iron oxides (secondary magnetite).

Mixed magnetite phases in the altered portion of the spinel (bright areas in BSE image, Fig. 5) generally fall under two groups. The first group includes magnetite and Cr-magnetite, which are rich in FeO_t, while the second group includes "ferritchromit" (Spangenberg, 1943), typically enriched in Cr_2O_3, TiO_2 and MnO. Replacement of Al-spinel (grey area in Fig. 5) by ferritchromit at the spinel rims (bright) occurs along the fractures and progressively affects the smaller Al-spinel grains. Ferritchromit also contain less FeO_t as compared to the magnetite.

We used the number of Fe^{3+} ions per X oxygens in the mineral formula, F=2X(1-T/S), where T is the ideal number of cations per formula unit and S is the observed cation total per X oxygens calculated assuming all iron to be Fe^{2+} (after Droop, 1987). Based on Cr# [Cr# = mole Cr/mole (Cr+Al)] and Mg# [Mg# = mole Mg/ mole ($Mg+Fe^{2+}$)], the spinels in NCIR serpentinised peridotites could be grouped into two categories (Fig. 6).

Group I: High Cr# (0.45-0.54) and low Mg# (0.57-0.68) variety, which are more abundant.

Group II: Low Cr# (~0.24-0.29) and high Mg# (0.72-0.77) variety, which are comparatively less abundant. In comparison to Group I spinels, characterised by variable Cr_2O_3 (38 to 44 wt %), Al_2O_3 (25 to 31 wt%), and MgO (12 to 16 wt %) content, Group II spinels have lower Cr_2O_3 (22-25 wt %), higher Al_2O_3 (45-48 wt %) and slightly higher MgO (18-19 wt %) content. TiO_2 content is also slightly higher (TiO_2 ~0.02 to 0.5 wt%) in Group I compared to Group II spinel (TiO_2 ~0.03-0.13 wt%). Fig. 7 shows the distribution pattern of TiO_2 content versus Cr# and Mg# for Group I and Group II spinels. Group II spinel characteristically have low TiO_2 (≤0.1 wt%) and for a given Cr#, they are comparable with spinel from other ridges (Fig. 7a). Mg# of Group I and Group II spinels are shown in Fig. 7b.

The Group I spinels are depleted in Al at their rims but enriched in Fe irrespective of variation in Cr content. A triangular plot (Fig. 8) for spinel interiors comprising both the groups (e.g. Cr rich and Cr poor) and the marginal areas (i.e. ferritchromit, Cr-magnetite and magnetite) shows that the two spinel groups distinctly occupy two different fields on Al-Cr line. The interrelation between FeO-TiO_2-Cr_2O_3 and MnO is further shown in Fig. 9. A progressive

decrease in Cr_2O_3 and MnO from ferritchromit zone to marginal magnetite zone (Fig. 9) is noted here. Group I spinel, occurring close to the gabbroic dikelets are often enriched in Ti content in comparison to those (Group II) occurring away from gabbroic dikelets (see Table 2, analyses # 5, 6). Ti content is also comparatively high in the margins of Group I spinel grains compared to their core (Fig. 2e). As mentioned earlier, Group I spinels with high Cr# (0.45-0.54) and low Mg# (0.57-0.69) are more abundant in the NCIR peridotites. Alteration of spinel and behaviour of elements during serpentinisation (i.e. enrichment or depletion) mainly account for their variability in Mg, Al, Cr and Fe contents, as shown in Fig. 10. Around relatively fresh domains of spinel, especially the core region, no substantial compositional changes are observed. The variability of Fe, Mg, Cr and Al are almost indistinguishable at core of the spinel. By contrast, Al decreases drastically at marginal areas (i.e. ferritchromit and magnetite-rich regions) while Fe increases from core to margin. Cr content almost maintains an uniform trend throughout the core and also in the adjacent ferritchromit zone.

Discussion

Degree of partial melting and melt-rock interaction

The differences in Cr# among the NCIR spinels suggest that the Group I spinels are more refractory than the Group II spinels (Fig. 6). As discussed later, the composition of Group I spinels have possibly been affected by interaction of Ti-rich evolved melt in the form of intrusion of mm to cm level thick gabbroic dikelets. To quantify the degree of melting of mantle peridotite, we have studied the mineral chemistry at the unaltered sectors of the intrusion-free Group II spinels. The findings indicate that apart from the petrographic evidences of absence of any gabbroic dikelets Group II spinel is characterised by very low Ti content (TiO_2 range between 0.03-0.13 wt%) to attest to their residual nature. Spinel in oceanic peridotite generally has low TiO_2 and high Fe^{2+}/Fe^{3+} compared with spinels from volcanic origin. Additionally, high Al_2O_3 in mid-ocean ridge spinel implies increasing Al activity in the system and this process reduces the partitioning of Ti into spinel (Kamenetsky et al., 2001). The high TiO_2 content in mantle peridotite is rather unusual and often corresponds to the presence of plagioclase and also implies that the trapped melt is TiO_2-rich (Dick, 1989; Hellebrand et al., 2002). Therefore, the low TiO_2 contents, irrespective of their low or high Cr contents of Group II spinels, suggest that the peridotites were never been in equilibrium with the intruding melt. Such low TiO_2

values are commonly considered as a characteristic of a plagioclase-free spinel peridotite that did not react with MORB liquid during low-pressure crystallization processes at shallow depth (Dick, 1989; Seyler and Bonatti, 1997).

Hellebrand et al. (2002) used a quantitative melting tool using the spinel compositions from the residual peridotites to estimate global variations in crustal thickness, and its dependence on spreading rate. In this study, to understand the empirical fractional melting function, the degree of melting is calculated by using the following equation after Hellebrand et al. (2002):

$$F = 10 \ln (Cr\#) + 24.$$

Considering the above equation for the Group II spinel (Cr# of 0.24), the NCIR peridotites indicate that they have undergone an intermediate degree of depletion that corresponds to ~10 % melting (see Fig. 6), which falls between most depleted mantle peridotite (~15%) and most fertile peridotite (~5%) reported from ocean ridge system. Our data on degree of partial melting, as inferred from spinel mineral chemistry further agrees well with those reported in the serpentinised peridotites from southern CIR (~ 13-15% of partial melting, Morishita et al., 2009).

Variability in spinel Cr# is not uncommon in oceanic peridotites. Substantial variations in Cr# (~0.17 to 0.29) were also reported earlier in serpentinised peridotites even from a single dredge haul from CIR (Hellebrand et al., 2002). More recently, Morishita et al. (2009) also studied peridotites from CIR and found spinel Cr# varies from 0.34 to 0.56. They correlated this finding with the size of the associated altered plagioclase and also with the occurrence of spinel corresponding to their distance from leucocratic veins (presently occupied by chlorite and or tremolite/ actonilite). Similarly in NCIR peridotites due to melt-spinel interaction, TiO_2 content of Group I spinel has increased adjacent to the gabbroic dikelets. Therefore, the variability in TiO_2 content in spinel of NCIR serpentinites is primarily due to the effect of intrusion of the gabbroic dikelets. As mentioned earlier, actinolite vein and spinel also occur at some places in close association with the late stage carbonate veins (Figs. 4 a,b,c). These web-like carbonate veins mainly imply non hydrothermal, low temperature seawater origin and are also common in other known ultramafic-hosted hydrothermal vent sites at MAR (cf. Ribeiro da Costa et al., 2008).

Condition of serpentinisation and spinel alteration

The occurrences of chlorite mostly as veins (often up to 10 vol%) within the serpentinised peridotites intruded by gabbroic dikelets suggest preexisting plagioclase feldspar were completely replaced by chlorite. The serpentine veins cross cutting the chlorite suggest alteration of plagioclase to chlorite occurred prior to main serpentinisation event. Otherwise, the formation of chlorite adjacent to spinel or in fractures within the large spinel grains is related to spinel alteration. The formation of chlorite due to spinel alteration was first described by Kimball (1990) and later modified by Mellini et al. (2005) as per following equation:

MAl_2O_4 + 1.5 $M_3Si_2O_5(OH)_4$ + H_2O + 0.083O_2
Al – spinel serpentine

= $M_5Al\ Si_3AlO_{10}(OH)_8$ + 0.167M_3O_4
chlorite Cr – magnetite

Thus, the close association of chlorite aureole at the spinel-ferritchromit grain boundary suggests that the spinel might have supplied the necessary Al, Mg and Cr contents for the formation of the chlorites. The secondary silicates are less accommodative of Mn than their precursors (Deer et al., 1992). In the absence of ilmenite and garnet, chrome-spinel is likely the favorable receptor for Mn, during serpentinisation. This may account for the observed high Mn-content at the ferritchromit zone (Fig. 9c). The associated serpentine minerals (mainly chrysotile and lizardite within serpentinites and chlorite-actinolite within the altered gabbroic dikelets) suggest that the alteration processes of NCIR peridotites might have occurred in two stages as follows:

(1) initially at relatively high temperature, gabbroic dikelets underwent alteration to chlorite-actinolite facies, which is evident by the presence of chlorite and actinolite veins and at a late stage (2) the main serpentinisation process resulted the formation of lizardite and chrysotile at relatively lower temperature. The formation of ferritchromit is probably synchronous with the bulk serpentinisation process, as their coexistence with the chlorite suggests their formation temperature is coeval with the greenschist facies. The bulk serpentinisation processes probably lasted long and superseded all events.

Generally the dark areas in the BSE image of the representative spinel grain (Fig. 5) are characterised with Mg-rich and Fe-poor composition, compared to the light colored altered rims

(with higher Fe^{2+}), due to the replacement of Mg^{2+} by Fe^{2+} in spinel structure during alteration. Mn-enrichment in the ferritchromit zones (Fig. 9c) might have occurred due to the possible interaction of hydrothermal fluids (Gahlan and Arai, 2007). To identify the alteration trend we have applied the following criteria: Zonation with a decrease in Mg, and Al contents and increasing Fe content towards the grain margins, which cannot be related to magmatic differentiation. This suggests that the alteration processes facilitate removal of Al and addition of Fe along the altered rim of the spinel grains and later a chemical reaction between the additional Fe and H_2O may have produced chlorite and ferritchromit. Due to highly immobile nature of Cr during alteration, any significant changes in Cr content are unlikely throughout the spinel grains. This is reflected both in fresh and altered areas of the spinel grains and shows while Cr_2O_3 content does not vary in any portion of the grain, rest of the elements (e.g. Mg, Al and Fe) varies to some extent. MgO and Al_2O_3 both are leached out from the altered portion, while FeO has been added during alteration (Fig. 10).

Conclusions

Based on our studies on NCIR serpentinites, following conclusions can be drawn:

1. Less abundant, plagioclase free residual spinel cores with low Ti content (Group II, Cr# ~ 0.24-0.25) retained its original composition despite high degree of serpentinisation of NCIR peridotite. Composition of more abundant Group I spinel have higher Cr# (~ 0.46-0.47) and TiO_2 content (up to 0.5 wt%).

2. The overall degrees of partial melting in these rocks correspond to ~10% (as obtained from Cr# of Group II spinel). This finding agrees well with the previous observations from other locations of CIR.

3. High TiO_2 particularly in Group I spinels, occurring adjacent to gabbroic dikelets, has resulted due to melt-rock interaction. Thus, the discrimination between residual peridotites and peridotites intruded by gabbroic dikelets is often reflected by the difference in their spinel TiO_2 contents.

4. The alteration of spinels resulted formation of intermediate ferritchromit zone and secondary magnetite at margins. Interiors of spinel porphyroclasts are generally fresh. During

alteration, Mg, Al leached out, but Cr did not change much, while Fe content increased resulting formation of secondary magnetite at marginal areas of spinel porphyroclast.

Acknowledgements

We thank Director, NIO, for permission to publish the manuscript. Ship time was provided by the Ministry of Earth Sciences, New Delhi. This research is partly funded by ONR grant no. 0014-97-1-0925 and partly by CSIR Network Programme (COR 0006). RB acknowledges INSA, New Delhi and JSPS, Tokyo for a fellowship to visit ORI, the University of Tokyo. We appreciate the help extended by the Captain, crew members and other colleagues, onboard ORV Sagar Kanya (cruise SK#195), during the sampling operations. DR is grateful to CSIR, New Delhi, for financial support in the form of a Senior Research Fellowship during the course of this research. Critical reviews by an anonynomous reviewer are greatly appreciated. This is NIO's contribution #…….

References

Arai, S. (1994) Characterization of spinel peridotites by olivine-spinel compositional relationships: review and interpretation. Chem. Geol., v. 113, pp. 191-204.

Bach, W., Garrido, C.J., Paulick, H., Harvey, J. and Rosner, M. (2004) Seawater-peridotite interactions: first insights from ODP Leg 209, MAR 15°N. Geochem. Geophys. Geosys., v. 5(9):Q09F26, doi:10.1029/2004GC000744.

Bach, W., Paulick, H., Garrido, C.J., Ildefonse, B., Meurer, W.P. and Humphris, S.E. (2006) Unraveling the sequence of serpentinization reactions: petrography, mineral chemistry, and petrophysics of serpentinites from MAR 15°N (ODP Leg 209, Site 1274). Geophys. Res. Letts., v. 33(13):L13306, doi:10.1029/2006GL025681.

Deer, W.E., Howei, R.A. and Zussman, J. (1992) The Rock Forming Minerals, second ed., Longmans, London.

Dick, H.J.B. and Natland, J.H. (1996) Late stage melt evolution and transport in the shallow mantle beneath the East Pacific Rise. Proc. Ocean Drill. Prog. Sci. Results, v. 147, pp. 103-13.

Dick., H.J.B. (1989) Abyssal peridotites, very slow spreading ridges and ocean ridge magmatism. Geol. Soc. Spec. Publ., v. 42, pp. 71-105.

Dick, H.J.B. and Bullen, T. (1984) Chromian spinel as a petrogenetic indicator in abyssal and alpine-type peridotites and spatially associated lavas. Contrib. Mineral. Petrol., v. 86, pp. 54-76.

Drolia, R.K., Iyer, S.D., Chakraborty, B., Kodagali, V., Ray, D., Misra, S., Andrade, R., Sarma, K.V.L.N.S., Rajasekhar, R.P. and Mukhopadhyay, R., (2003) The Northern Central Indian

Ridge: Geology and tectonics of fracture zones-dominated spreading ridge segments. Curr. Sci., v. 85, pp. 290-298.

Drolia, R.K. and DeMets, C. (2006) Deformation in the diffuse India-Capricorn-Somalia triple junction from a multibeam and magnetic survey of the northern Central Indian ridge, 3ºS-10ºS. Geochem. Geophys. Geosyst., v.6:Q09009, doi: 10.1029/2005GC00950

Droop, G.T.R. (1987) A general equation for estimating Fe^{3+} concentrations in ferromagnesian silicates and oxides from microprobe analyses, using stoichiometric criteria. Mineral Mag., 51, 431-435.

Engel, C.G. & Fisher, R.L. (1975). Granitic to ultramafic rock complexes of the Indian ocean ridge system, Western Indian Ocean. *Geological Society of America Bulletin* 82, 553-562.

Gahlan, H.A. and Arai, S. (2007) Genesis of peculiarly zoned Co, Zn and Mn-rich chromian spinel in serpentinite of Bou-Azzer ophiolite, Anti-Atlas, Morocco. J. Min. Petrol. Sci., v. 102, pp. 69-85.

Ghose, I., Cannat, M. and Seyler, M. (1996) Transform fault effect on the mantle melting in the MARK area (Mid-Atlantic Ridge south of the Kane transform). Geol., v. 24, pp.1139-1142.

Hellebrand, E.W., Snow, J.E., Hoppe, P., Hofmann, A.W. (2002) Garnet-field melting and late- stage refertilisation in 'residual' abyssal peridotites from the Central Indian Ridge. J. Petrol., v. 43, pp. 2305-2338.

Kamesh Raju, K.A., Samudrala, K., Drolia, R.K., Amarnath, D., Ramachandran, R., and Mudholkar, A. (2012) Segmentation and morphology of the Central Indian Ridge between 3°S and 11°S, Indian Ocean. Tectonophys., v. 554, pp. 114-126.

Kamenetsky, V.S., Crawford, A.J. and Meffre, S., 2001. Factors controlling chemistry of magmatic spinel: an empirical study of associated olivine, Cr-spinel and melt inclusions from primitive rocks. J Petrology, 42, 655-671.

Kimball, K.L. (1990) Effects of hydrothermal alteration on the composition of chromium spinels. Contrib. Mineral. Petrol., v. 105, pp. 337–346.

Morishita, T., Hara, K., Nakamura, K., Sawaguchi, T., Tamura, A., Arai, S., Okino, K., Takai, K. and Kumagai, H. (2009) Igneous, alteration and exhumation processes recorded in abyssal peridotites and related fault rocks from an oceanic core complex along the Central Indian Ridge. J. Petrol., v. 50, pp.1299-1325.

Mahoney, J.J., Roex, A.P., Peng, Z., Fisher, R.L. and Natland, J.H. (1989) Southwestern limits of the Indian Ocean Ridge mantle and the origin of low $^{206}Pb/^{204}Pb$ mid-ocean ridge basalts: Isotopic systematic of the central Southwest Indian Ridge (17-50E). J. Geophys. Res., v. 97, pp. 4033-4052.

Mellini, M., Rumori, C. and Viti., C. (2005) Hydrothermally reset magmatic spinels in retrograde serpentinites: formation of "ferritchromit" rims and chlorite aureoles. Contrib. Mineral. Petrol., v. 149, pp. 266-275.

Natland, J.H. (1991) Indian ocean crust. In: Floyd PA (ed) *oceanic basalts*. Blackie and Sons, Glasgow, pp. 289-310.

Ray, D., Iyer, S.D., Banerjee, R., Misra, S. and Widdowson, M. (2007) Petrology and Geochemistry of basalts from the Northern Central Indian Ridge (3-11ºS): implications for the evolution of MORB. Acta Geol. Sin. (English version), v. 81, v. 99-112.

Ray, D., Banerjee, R., Iyer, S.D. and Mukhopadhyay, S. (2008). A new report of serpentinites from Northern Central Indian Ridge – an implication for hydrothermal activity. Acta Geol. Sin. (English version), v. 82, v. 1213-1222.

Ray, D., Misra. S., Banerjee, R. and Weis, D. (2011) Geochemical implications of gabbro from slow-spreading Northern Central Indian Ocean Ridge, Indian Ocean. Geol. Mag., v. 148(3), pp. 404-422.

Ray, D., Misra, S. and Banerjee, R. (2013) Geochemical variability of MORBs along slow to intermediate spreading Carlsberg-Central Indian Ridge, Indian Ocean. J. Asian Earth Sciences, v. 70-71, pp. 125-141.

Rehkämper, M. and Hofmann, A.W. (1997) Recycled ocean crust and sediment in Indian Ocean MORB. Earth Planet Sci. Lett., v. 78, pp. 379-396.

Ribeiro da Costa, I., Barriga F.J.A.S. and Taylor, R.N. (2008). Late seaflooe carbonate precipitation in serpentinites from the Rainbow and Saldhana sites (Mid-Atlantic Ridge). Eur J. Mineral., 20, 173-181.

Ross, K. and Elthon, D. (1997) Extreme incompatible trace element depletion of diopside in residual mantle from south of the Kane Fracture Zone. Proc. Ocean Drill. Prog. Sci. Results, v. 153, pp. 277-284.

Seyler, M., Cannat, M. and Mevel C (2003) Evidence for major-element heterogeneity in the mantle source of abyssal peridotites from the Southwest Indian Ridge (52º to 68ºE). Geochem. Geophys. Geosyst., v. 4. doi: 10.1029/2002GC000305.

Spangenberg, K. (1943) Die Chrotlagerstatte von Tampadel am Zobten. Zietschr Prakt. Geol., v. 5, pp.13-25.

Seyler, M., Bonatti, E. (1997) Regional-scale melt-rock interaction in lherzolite mantle in the Romanche fracture zone (Atlantic Ocean). Earth. Planet. Sci. Letts., v. 146, pp. 273-287

Table Captions

Table 1. Brief petrographic descriptions of two spinel groups.

Table 2. Representative microprobe analyses of spinels from NCIR.

Table 3. Comparative spinel compositions from world's mid ocean ridge system (after Hellebrand et al., 2002).

Figure Captions

Fig. 1. Sampling location on the NCIR. Filled square represents the dredge location, south of the Vityaz TF at ridge-transform intersection (RTI). Thinner lines represent the TF and thicker lines are ridge segment. CR~ Carlsberg Ridge, NCIR~ Northern Central Indian ridge, CIR~ Central Indian Ridge, RTJ~ Rodriguez Triple Junction, SWIR~ Southwest Indian Ridge and SEIR~ Southeast Indian Ridge. Depth contour map scale 1: 5000000.

Fig. 2. Photomicrographs of different spinel grains:

a) Fractured spinel grains with fresh inner core. Along the fractures chloritisation (Chl) took place. Rims altered to magnetite (Mag) (sample no II-A).

b) Serpentinisation (Serp) took place along the fractured spinel grains (sample no II-A).

c) Mushroom shaped spinel porphyroclast within serpentine mesh rim (sample no. I-B).

d) Spinel as stringers within serpentine mesh rim (sample no I-B).

e) Spinel adjacent to thin actinolite vein (sample no. I-E)

f) Chlorite vein intrudes the bastite (sample no. I-F)

All photographs are under crossed polarized light (scale bar 1 mm).

Fig. 3. Typical (a) 'mesh' and (b) 'bastite' texture of NCIR serpentinite.

Fig. 4a. Late carbonate veins postdate the 'bastite', b. BSE image and c. X-ray mapping for C of carbonate vein

Fig. 5. Back scatter Electron (BSE) Image of spinel porphyroclast. Dark areas are fresh spinel (Sp) while brighter areas are altered portions with secondary magnetite (Mt) replacing spinel.

Fig. 6. Mg# plotted against Cr# in spinels from NCIR along with spinels from different ocean ridge settings (see Table 3). Degree of melting at different settings are also calculated using equation 1 and plotted at the right hand side.

Fig. 7. TiO_2 plotted against a. Cr# and b. Mg#. Two different groups of spinel (Group I and II) and range of TiO_2 content for depleted peridotite and gabbro impregnated peridotite also shown. Spinel from CIR, MARK and SWIR also incorporated for comparison.

Fig. 8. Ternary plot of Al-Cr-Fe^{2+} (all calculated in atoms per formula unit). Spinel I and Spinel II lie as two different cluster on Al-Cr line. Altered spinel grains analyses lie on Cr-Fe^{2+} line with an increasing Fe^{2+} trend as alteration increases.

Fig. 9. Binary plot of FeO_t vs a. Cr_2O_3%, b. TiO_2 % and c. MnO% to discriminate ferrit-chromit and Magnetite (or Cr-magnetite).

Fig. 10. Compositional variations of four major oxides (Cr_2O_3, MgO, Al_2O_3 and FeO_t) along line A-A' (Fig. 5) within a spinel porphyroclast:

(a) MgO and (c) Cr_2O_3 content (wt%) highest in spinel and fall gradually from

(e) ferritchromit to (g) magnetite.;

(b) Al_2O_3 content (wt%) is highest in fresh spinel, and (f) variable in ferritchromit;

(d) FeO_t content (wt%) is lowest in fresh spinel; but (h) is highest within magnetite.

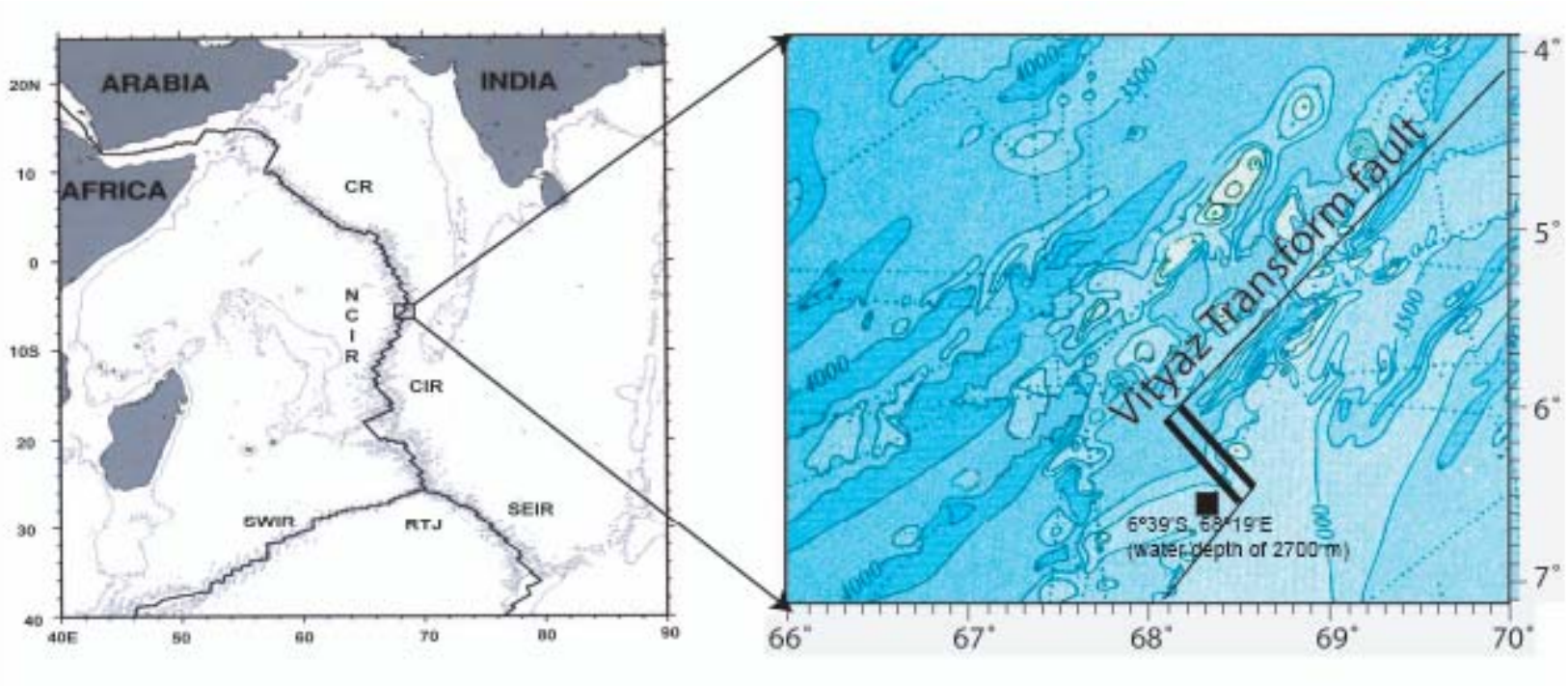
ARABIA
INDIA
AFRICA
CR
NCIR
CIR
SWIR
RTJ
SEIR
20N
10
0
10S
20
30
40
40E
50
60
70
80
90
Vityaz Transform fault
6°39'S, 68°19'E
(water depth of 2700 m)
4°
5°
6°
7°
66°
67°
68°
69°
70°

Figure-1

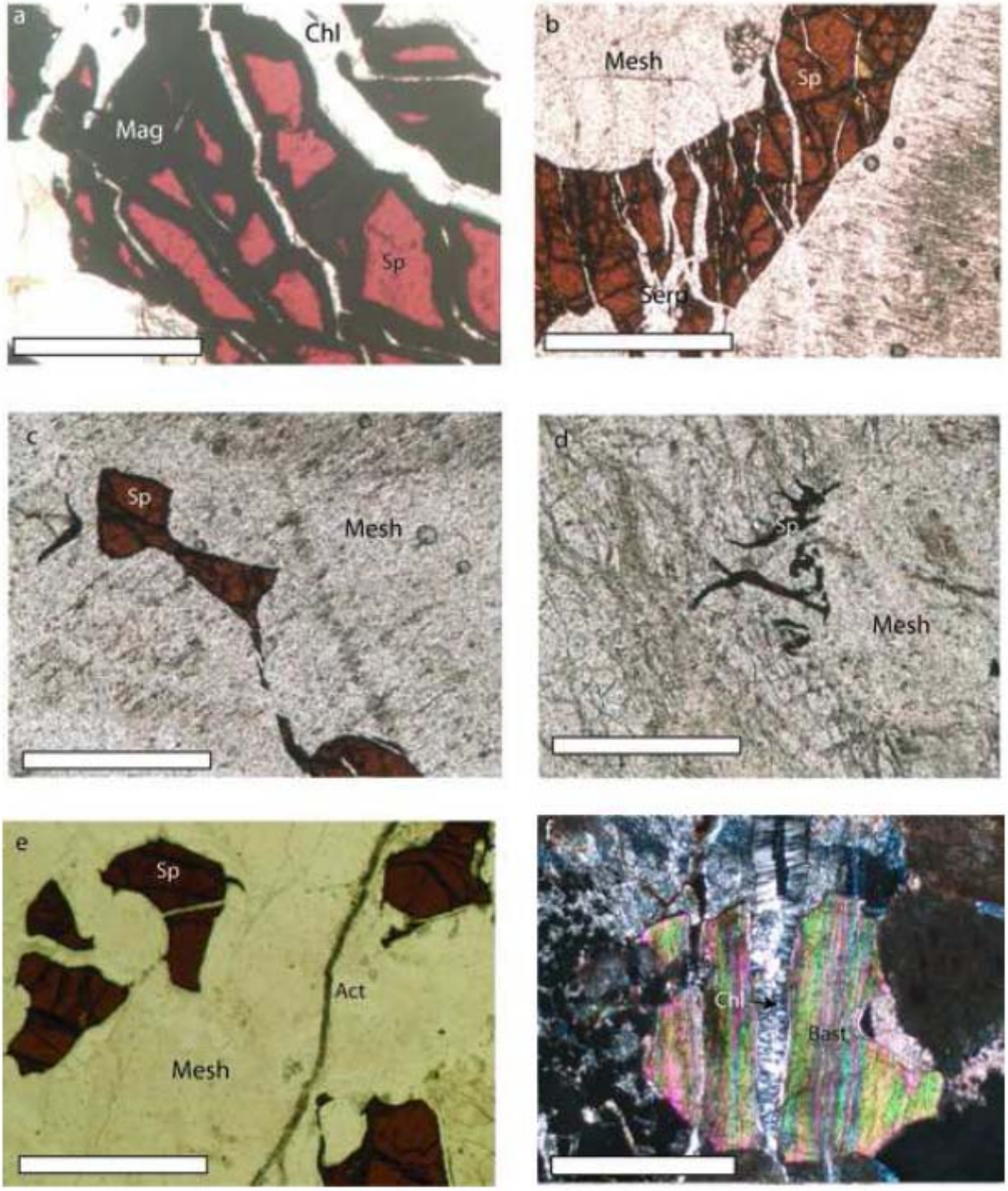
a
Chl
Mag
Sp
b
Mesh
Sp
Serp
c
Sp
Mesh
d
Sp
Mesh
e
Sp
Act
Mesh
Chl
Bast

Figure-2

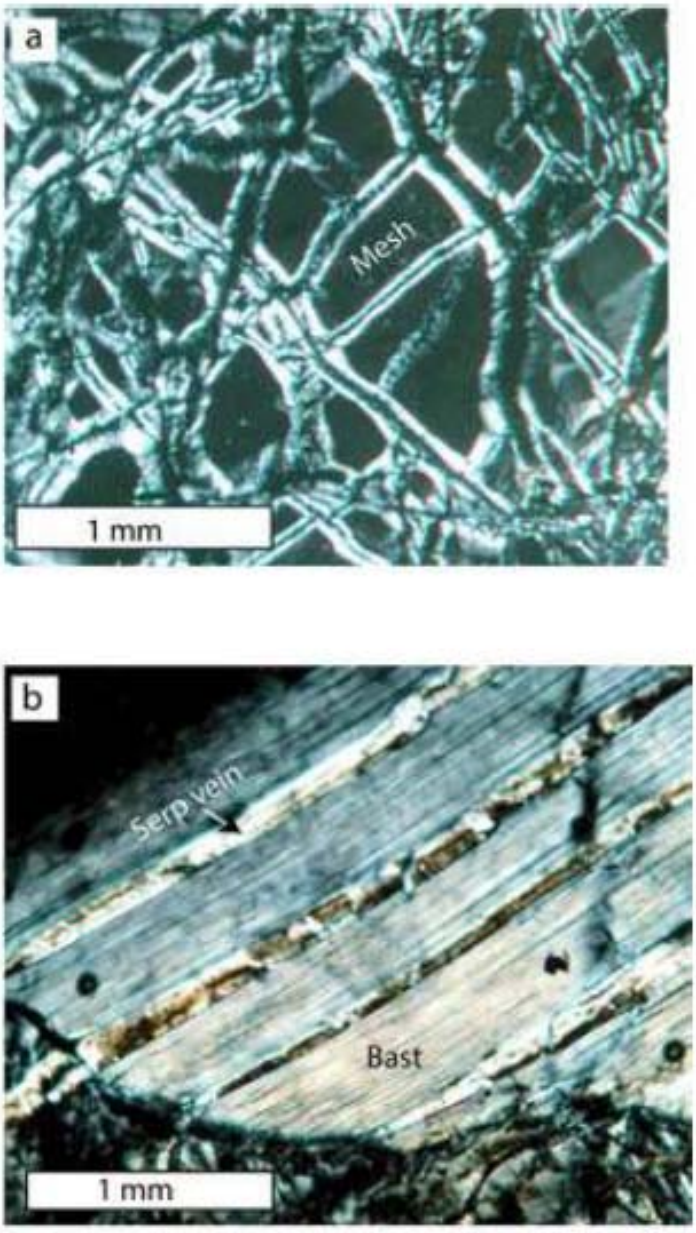

Figure-3

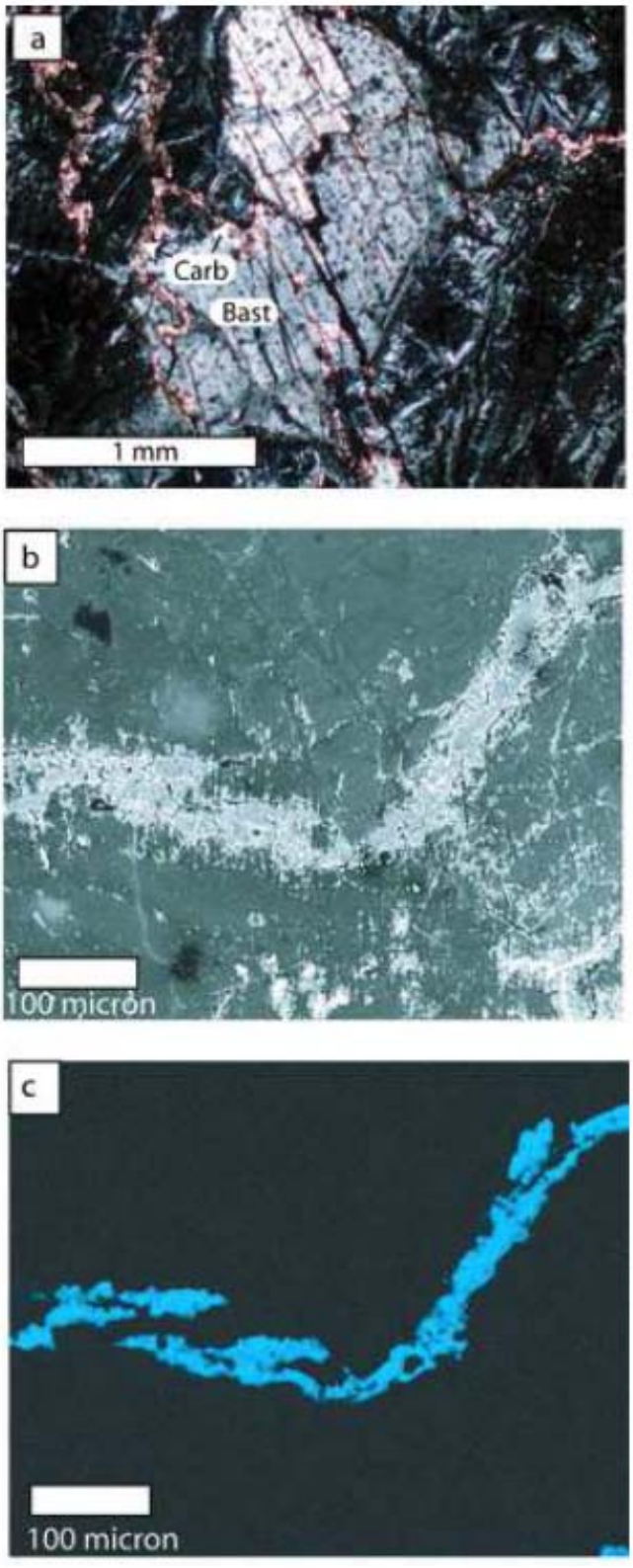

Figure-4

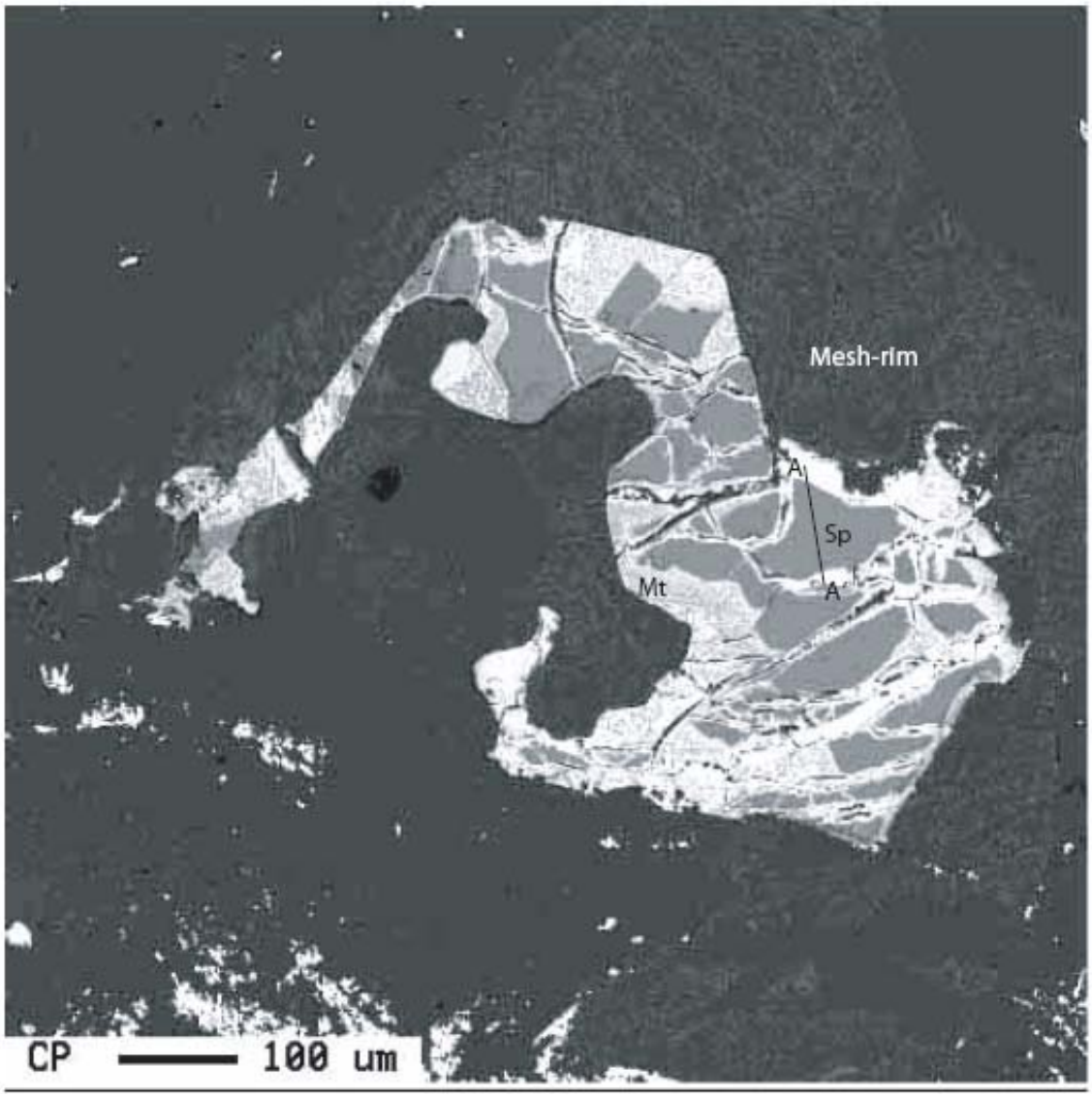

Figure-5

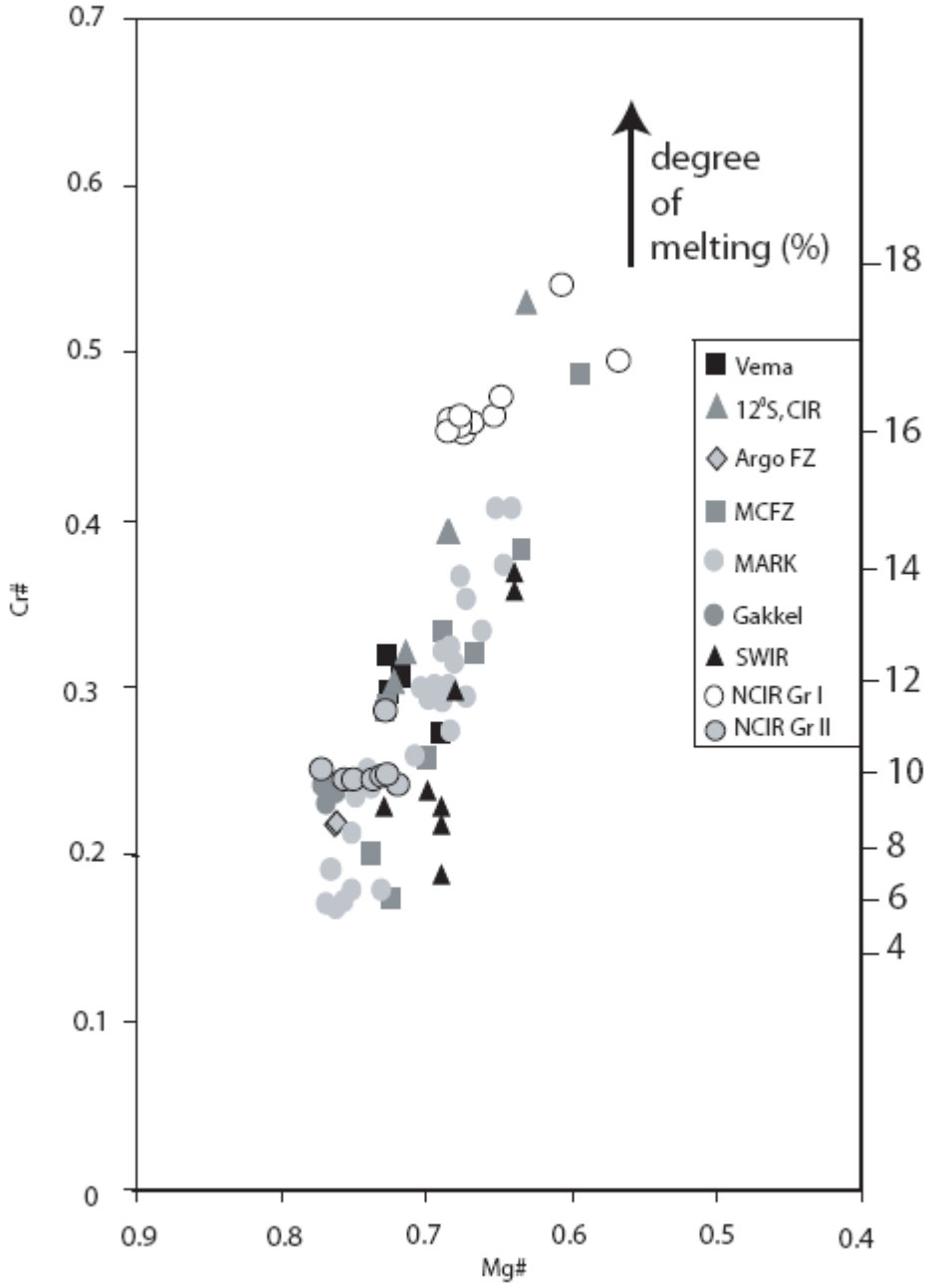
0.7
0.6
0.5
0.4
0.3
0.2
0.1
0
Cr#
0.9
0.8
0.7
0.6
0.5
0.4
Mg#
degree
of
melting (%)
18
16
14
12
10
8
6
4
Vema
12°S, CIR
Argo FZ
MCFZ
MARK
Gakkel
SWIR
NCIR Gr I
NCIR Gr II

Figure-6

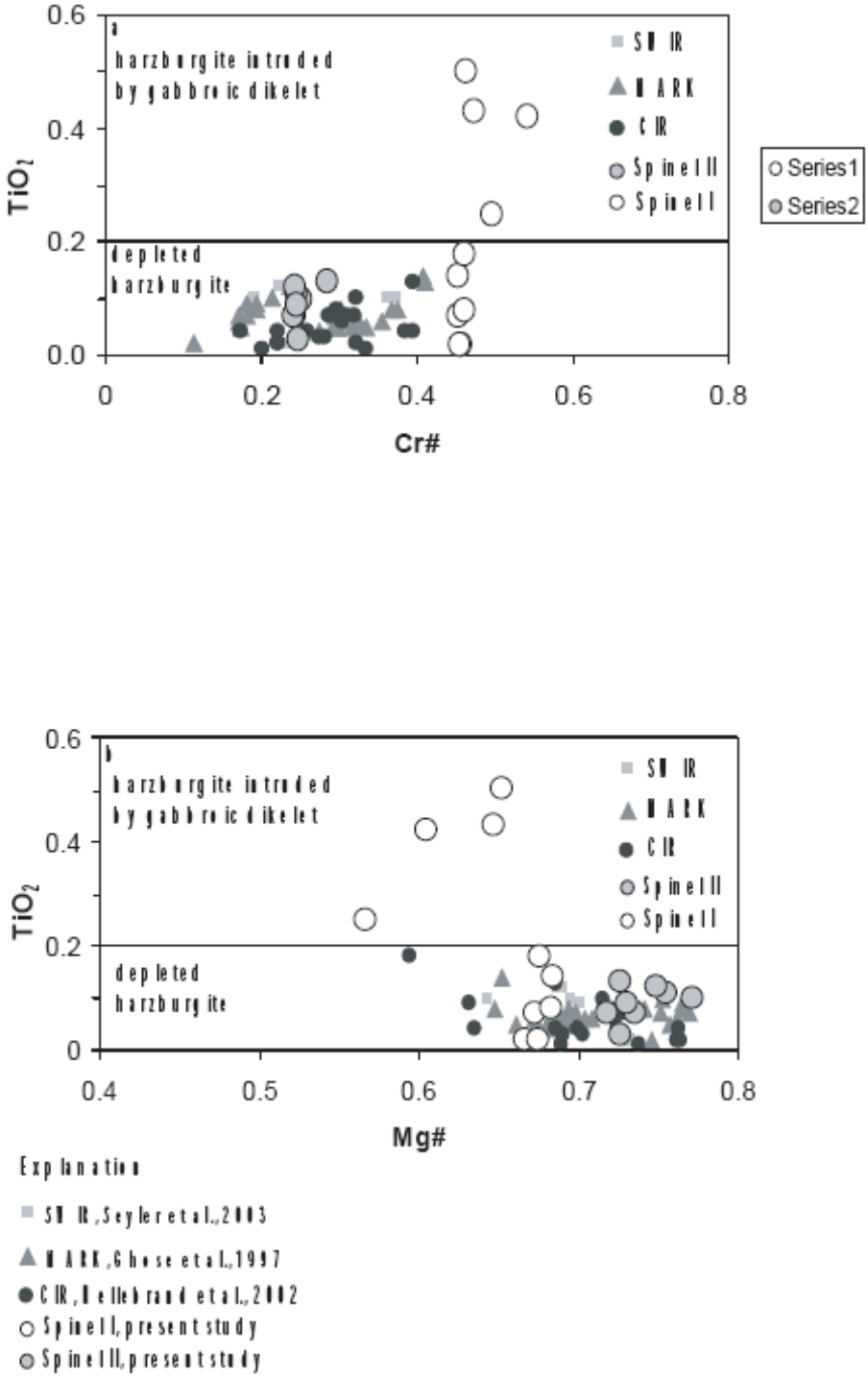
a
harzburgite intruded
by gabbroic dikelet
depleted
harzburgite
SWIR
MARK
CIR
Spinel II
Spinel I
Series1
Series2
TiO2
Cr#
0.6
0.4
0.2
0.0
0
0.2
0.4
0.6
0.8
b
harzburgite intruded
by gabbroic dikelet
depleted
harzburgite
SWIR
MARK
CIR
Spinel II
Spinel I
TiO2
Mg#
0.6
0.4
0.2
0
0.4
0.5
0.6
0.7
0.8
Explanation
SWIR, Seyler et al., 2003
MARK, Ghose et al., 1997
CIR, Hellebrand et al., 2002
Spinel I, present study
Spinel II, present study

Figure-7

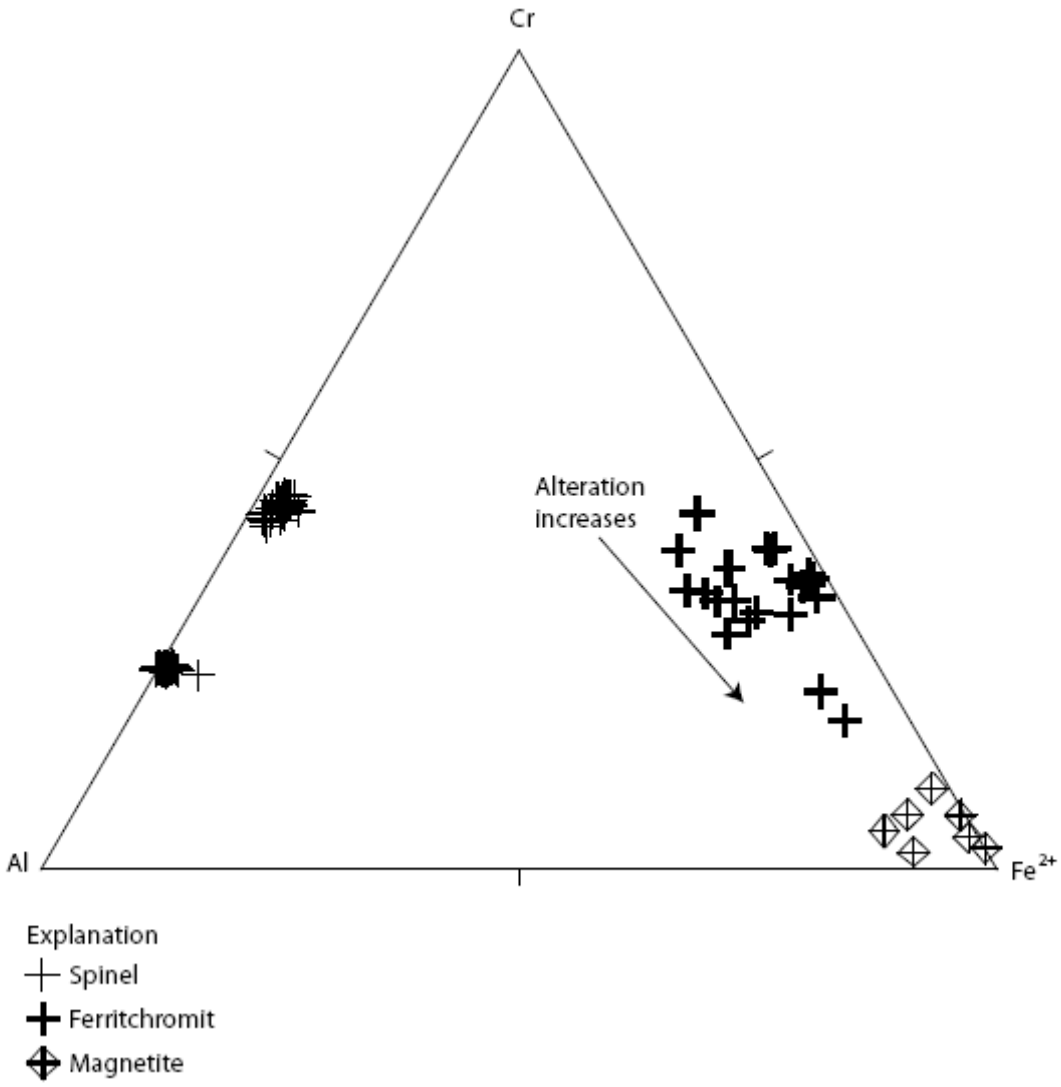
Cr
Alteration
increases
Al
Fe2+
Explanation
Spinel
Ferritchromit
Magnetite

Figure-8

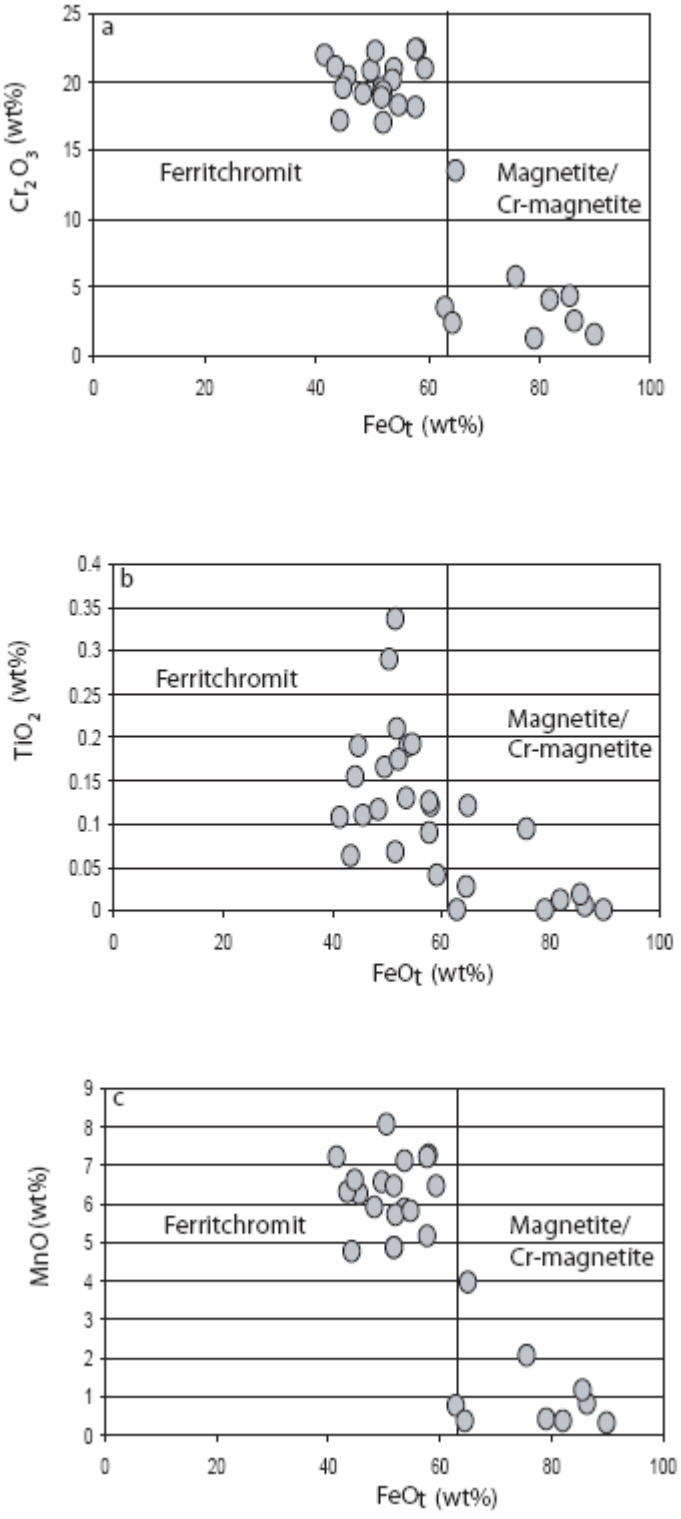
a
Ferritchromit
Magnetite/
Cr-magnetite
Cr_2O_3 (wt%)
FeOt (wt%)
b
Ferritchromit
Magnetite/
Cr-magnetite
TiO_2 (wt%)
FeOt (wt%)
c
Ferritchromit
Magnetite/
Cr-magnetite
MnO (wt%)
FeOt (wt%)

Figure-9

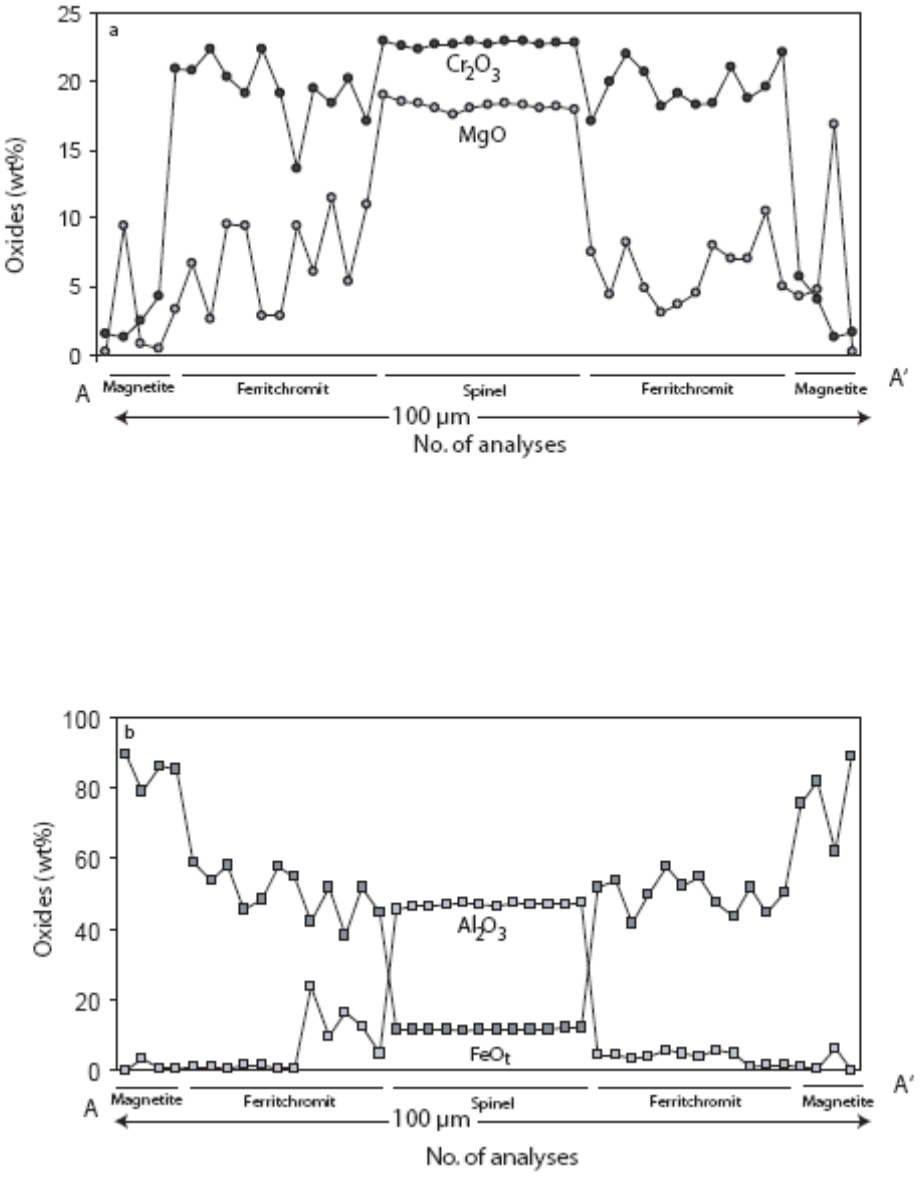
a
Cr_2O_3
MgO
Oxides (wt%)
25
20
15
10
5
0
A
Magnetite
Ferritchromit
Spinel
Ferritchromit
Magnetite
A'
100 µm
No. of analyses
b
Al_2O_3
FeO_t
Oxides (wt%)
100
80
60
40
20
0
A
Magnetite
Ferritchromit
Spinel
Ferritchromit
Magnetite
A'
100 µm
No. of analyses

Figure-10

Table 1

	Original lithotype of samples	Mineralogy	Alteration state
Group I Spinel (n=10)	Harzburgite and harzburgite impregnated by gabbroic dikelet	Serpentine mesh or veins, Opx bastite, magnetite, spinel occurs as skeletal, porphyroclasts. Plagioclase of gabbro pseudomorphed to chlorite. Ilmenite, apatite also present within gabbro locally. Acicular actinolite also occurs as veins. Mesh, opx 'bastite' and a few olivine within harzburgite.	85-95%
Group II Spinel (n=5)	Harzburgite	Serpentine mesh or veins, Opx bastite, abundant magnetite dust rimming the mesh rim. Euhedral and subhedral spinel grains. Fresh olivine rare.	90-100%

n=no. of samples

Table

Table 2

	Group I									
Sample nos	I-A	I-B	I-C	I-D	I-E	I-F	I-G-1	I-G-2	I-H-1	I-H-2
	within serpentinite	within serpentinite	within serpentinite	within serpentinite	close to gabbroic dikelet	close to gabbroic dikelet	close to gabbroic dikelet rim	close to gabbroic dikelet core	close to gabbroic dikelet rim	close to gabbroic dikelet core
SiO_2	0.03	0.01	0.03	0.05	0.03	0.01	0.05	0.05	0.05	0.02
TiO_2	0.07	0.02	0.08	0.02	0.50	0.43	0.25	0.14	0.42	0.18
Cr_2O_3	38.23	38.52	38.41	37.87	38.54	39.43	39.94	36.69	43.78	39.57
Al_2O_3	31.07	30.44	30.23	30.34	30.04	29.42	27.26	29.71	24.93	30.94
MgO	15.45	15.26	15.65	15.42	14.89	14.84	12.31	15.22	13.39	15.70
FeO_t	15.07	15.75	15.55	16.04	15.01	15.96	17.02	15.23	16.44	14.54
CaO	n.d.	n.d.	0.01	n.d.	0.02	0.03	n.d.	0.17	0.01	n.d.
MnO	0.15	0.12	0.20	0.19	0.14	0.13	0.08	0.21	0.21	0.13
Na_2O	n.d.	0.01	0.02	0.03	0.01	0.02	0.03	0.00	0.01	0.02
K_2O	n.d.	n.d.	n.d	n.d.	n.d.	0.01	n.d.	0.03	n.d.	0.01
Total	100.07	100.12	100.17	99.95	99.17	100.28	96.94	97.45	99.24	101.11
	Cations based on 32 oxygens									
Si	0.007	0.003	0.006	0.011	0.007	0.002	0.012	0.012	0.013	0.005
Ti	0.012	0.003	0.014	0.003	0.089	0.076	0.047	0.003	0.070	0.031
Al	8.607	8.471	8.404	8.461	8.426	8.217	7.990	8.481	7.199	8.480
Cr	7.101	7.148	7.161	7.083	7.248	7.384	7.849	7.023	8.478	7.273
Fe_t	2.961	3.109	3.067	3.173	2.985	3.163	3.539	3.084	3.368	2.827
Mn	0.03	0.024	0.039	0.038	0.027	0.027	0.016	0.043	0.043	0.025
Mg	5.411	5.367	5.501	5.437	5.278	5.239	4.561	5.493	4.889	5.439
Ca	n.d.	0.001	0.002	0.001	0.006	0.007	n.d.	0.043	0.002	0.001
Na	n.d.	0.002	0.009	0.012	0.003	0.01	0.013	0.001	0.004	0.008
K	0.001	n.d.	n.d.	n.d.	n.d.	0.002	n.d.	0.010	n.d.	0.003
Catsum	24.13	24.128	24.203	24.219	24.069	24.127	24.027	24.193	24.066	24.092
Fe^{3+}	0.34	0.44	0.52	0.56	0.18	0.32	0.05	0.55	0.19	0.23
Cr#	45.21	45.76	46.01	45.57	46.24	47.33	49.56	45.30	54.08	46.17
Mg#	67.38	66.82	68.4	67.6	65.31	64.84	56.7	68.52	60.62	67.7

n.d. not determined
Cr# : mole Cr/mole(Cr+Al); Mg#: mole Mg/ mole (Mg+Fe^{2+}). Fe^{2+} is calculated using spinel stoichiometry

Table 2 contd….

	Group II							
Sample nos	II-A within serpentinite	II-B within serpentinite	II-C within serpentinite	II-D within serpentinite	II-E within serpentinite	II-F within serpentinite	II-G within serpentinite	II-H within serpentinite
SiO_2	0.01	0.04	0.03	0.01	0.05	0.02	n.d.	0.04
TiO_2	0.10	0.11	0.12	0.07	0.07	0.09	0.13	0.03
Cr_2O_3	22.97	22.56	22.42	22.70	22.67	23.00	24.66	22.50
Al_2O_3	45.86	46.50	46.38	46.94	47.59	47.11	44.58	45.74
MgO	19.06	18.58	18.45	18.09	17.64	18.09	17.71	17.57
FeO_t	11.44	11.82	11.73	11.80	11.25	11.75	12.28	12.11
CaO	n.d.	n.d.	n.d.	n.d.	0.01	n.d.	n.d.	0.02
MnO	0.13	0.29	0.17	0.16	0.26	0.12	0.18	0.13
Na_2O	0.01	0.01	n.d.	0.04	n.d.	n.d.	n.d.	0.03
K_2O	0.01	n.d.	0.01	0.01	n.d.	0.01	n.d.	n.d.
Total	99.60	99.90	99.31	99.83	99.53	100.19	99.54	98.16
	Cations based on 32 oxygens							
Si	0.002	0.008	0.006	0.002	0.01	0.005	n.d.	0.008
Ti	0.017	0.018	0.019	0.011	0.011	0.015	0.021	0.005
Al	11.8	11.929	11.959	12.041	12.201	12.035	11.401	11.970
Cr	3.964	3.881	3.877	3.905	3.898	3.94	4.574	3.947
Fe	2.088	2.152	2.145	2.148	2.046	2.13	2.228	2.247
Mn	0.024	0.053	0.032	0.03	0.047	0.022	0.034	0.024
Mg	6.201	6.025	6.016	5.867	5.716	5.844	5.728	5.813
Ca	n.d.	n.d.	0.001	0.001	0.002	n.d.	n.d.	0.004
Na	0.004	0.005	n.d.	0.017	n.d.	n.d.	n.d.	0.012
K	0.003	n.d.	0.002	0.003	n.d.	0.002	n.d.	0.008
Catsum	24.103	24.071	24.057	24.025	23.931	23.993	23.986	24.038
Fe^{3+}	0.26	0.21	0.15	0.05	n.d.	n.d.	0.09	0.07
Cr#	25.15	24.55	24.48	24.49	24.21	24.66	28.63	24.79
Mg#	77.27	75.69	75.09	73.65	71.94	73.13	72.81	72.76

n.d. not determined

Table

Table 3

Ridge System	Location	Dredge/ Drill hole	Rock type	No. of analyses	Cr#		Mg#	
				N	Avg	Range	Avg	Range
Northern CIR[1]	Off-ridge axis	Dredge 5º37'S	Serpentinite	38 64	25 46	24-25 43-47	73 64	72-75 60-66
CIR[2]	Axial valley	Dredge 12ºS	Serpentinised lherzolite	5	39	31-53	69	63-72
	Vema TF	Dredge 8º42'S	Serpentinised lherzolite	4	30	27-32	72	69-73
	Argo TF	Dredge 13º34'S	Lherzolite, Serpentinite	3	22	------	76	-------
	Marie celeste TF	Dredge 17º38'S	Orthopyroxenite, lherzolite, Serpentinite	10	30	17-49	69	59-74
MAR[3]	MARK	ODP site 920	Serpentinised harzburgite and lherzolite	115	29	28-31	71	70-72
SWIR[4]	Axial valley	Dredge 52-68ºE	Spinel lherzolite/ Harzburgite	8	27	19-37	68	64-73
EPR[5]	Hess Deep	ODP site 895	Dunite, Harzburgite	88	64	52-70	54	48-61
Gakkel Ridge[2]	Off-ridge axis	Dredge 22º43'E	Serpentinite	4	24	23-25	77	76-77

1.Present study; 2. Hellebrand et al.(2002); 3. Ross and Elthon (1997);
4. Seyler et al.(2003); 5. Dick and Natland (1996).